EFFECT OF THERMAL GRADIENT ON WELD STRENGTH IN FUSED FILAMENT FABRICATION

Ferrarotto, N[1] and Hubert, P[1,2]*
[1] Department of Mechanical Engineering, McGill University, Montreal, Canada
[2] Research Center for High Performance Polymer and Composite Systems (CREPEC)
* Corresponding author (pascal.hubert@mcgill.ca)

Keywords*: thermal imaging, additive manufacturing, first article inspection*

ABSTRACT

Fused filament fabrication (FFF) has seen rapid growth in recent years thanks to the development of machines and materials able to compete with traditional processes (injection, compression moulding, etc.) on a cost and performance basis. The aerospace industry is now looking to produce structural components using this technique. Such components are typically certified through first article inspection (FAI) where the first parts produced are used as witness samples for mechanical testing. Subsequent production requires consistent processing conditions to result in equally strong parts. The objective of this paper is to develop a framework to evaluate the consistency of processing conditions in FFF via process monitoring. Interlayer tensile strength (or weld strength) is identified as a critical property of printed parts which is highly dependent on process conditions. An experiment is conducted to evaluate the effect of 5 parameters (nozzle temperature, chamber temperature, print speed, layer width and layer height) on the weld strength of ASTM D638 Type I coupons printed in the vertical (Z-axis) direction. In a parallel experiment, the consistency of processing conditions is evaluated by monitoring the thermal gradient during material deposition. It was found that shorter layer times caused steeper thermal gradients which in turn resulted in higher inter-layer weld strength.

1 INTRODUCTION

The main hurdle currently faced by fused filament fabrication (FFF) in aerospace is certification. Before seeing such parts in our airplanes, adequate procedures must be laid out to ensure they perform as well as those made using traditional methods. Since failure requirements such as tensile strength can only be verified through part destruction, the quality of parts for commercial use must be demonstrated to perform equally well as those tested by the manufacturer. In a method called first article inspection (FAI), the first parts produced are used as witness samples for mechanical testing while the remaining are sold to customers. Production requires consistent processing conditions to result in equally strong parts. Currently, such consistency with FFF is readily achievable only with expensive proprietary machines.

There is a challenge in wanting to make an open source FFF machine perform as well as a proprietary one. The machine must be carefully selected to ensure its hardware has the potential to produce parts with desired repeatability. Open-source manufacturers often need to work around patent-protected features which could enhance print quality, speed, or reliability. This may include embedded sensors allowing printers to self-correct to minimize geometrical or thermal deviations. This paper aims to use infrared thermography to establish a link between process parameters and resulting inter-layer properties. The industry has yet to develop certification standards for FFF parts and must resort to systematic mechanical testing. Proper sensing capabilities could dramatically reduce the amount of necessary testing and associated production costs.

2 BACKGROUND AND OBJECTIVE

At its core, FFF consists of a nozzle extruding thermoplastic filament in a highly controlled manner. Material is deposited onto a build plate in the form of a bead (or raster). Juxtaposed beads form layers which successively stack on top of one another. The initial layer adheres directly to the build plate while subsequent layers bond to the one below them. The thicknesses of each layer add up, giving the final part its height.

2.1 Process Parameters

Process parameters (also called print settings or profiles) are defined by the user in the slicing software (or slicer) and fed to the printer via G code. The following were selected as especially relevant to understanding the FFF process and the scope of this work.

This work was mainly concerned with extrusion settings which largely depend on material selection. The nozzle temperature must be set above the filament's melting point to ensure consistent extrusion with minimal back pressure. Excessive pressure in the hot end resulting from incomplete melting or high melt viscosity can cause slippage of the extruder gears, leading to under-extrusion. Nozzle temperature is typically provided by filament suppliers to be used as a starting point for experimental fine-tuning.

Once the optimal nozzle temperature has been determined, the flow rate (or extrusion multiplier) can be determined and set. The flow rate is a percentage representing the number of motor steps needed to extrude a given length of filament. The default flow rate is 100%. A higher valuer (e.g., 105%) can be set to compensate for under-extrusion and vice-versa for over-extrusion.

When printing the bulk of the part, extrusion width is typically set as equal to the nozzle diameter or slightly higher to accommodate induced die swelling. Increasing the extrusion width will decrease the total number of beads in a single layer rather than pack them tighter (the latter is done by increasing the flow rate). It can be tuned to fill gaps in thin walls and match the geometry defined in CAD.

Layer height defines the increment by which the nozzle-bed distance increases before printing a new layer. It does not affect how much the bead is "squished" (again, this is affected by the flow rate). It does however affect the amount of shear stress developed inside the deposited bead which may affect inter-layer bonding characteristics. Layer height has a direct effect on print time and resolution. For example, bringing it down from 0.2 mm to 0.1 mm will double the Z-axis resolution of the part, but also double the print time since there will be twice as many layers to print.

Layer time is simply the time required to print a layer of material. It mainly depends on layer size, toolpath, print speed, and acceleration. Layer time control is critical in large-scale AM where cooldown management plays a significant role in process optimization. Compton et al. [1] specifically varied layer time to find the optimal setting long enough to avoid warping and short enough to avoid cracking. In metal wire feed AM, layer time is a critical parameter due to its impact on thermal gradient [2]. There appears to be less emphasis on layer time in conventional scale FFF research.

Any variation in temperature with respect to space is known as a thermal gradient. Thermal gradients are a driving force of heat transfer. In FFF, the traveling toolhead creates a significant thermal gradient between the polymer melt being deposited and the layers beneath it. As a result, this temperature variation dictates the rate at which the extruded material solidifies into a rigid bead. Toolpath and geometry cause the thermal gradient to also vary in time. In larger geometries, longer layer times allow increased cooldown between passes. As a result, wider variations in thermal gradient can occur. Because of its influence on the rate of solidification, the thermal gradient created from successive layer deposition and solidification is hypothesized to impact the degree of coalescence and bonding between layers. This would imply a significant correlation between measured thermal gradient and inter-layer mechanical properties.

Like layer time, thermal gradient is not explicitly controlled in the printing process. Instead, it varies as a function of the slicer settings and environmental conditions. Given the mathematical formulation of the diffusion of heat, where T is temperature, t is time, α is the thermal diffusivity constant, and x, y and z are spatial variables,

$$\frac{1}{\alpha}\frac{\partial T}{\partial t} = \frac{\partial^2 T}{\partial x^2} + \frac{\partial^2 T}{\partial y^2} + \frac{\partial^2 T}{\partial z^2} \tag{1}$$

it is natural to expect said diffusion to depend on parameters related to time, space and temperature. The specific parameters expected to affect the thermal gradient during layer deposition are thus layer time, print speed, layer height, extrusion width, as well as temperatures of the nozzle, chamber, and bed. It is hypothesised that layer time will have a significant effect on interlayer thermal gradient as it captures the effect of geometry and print speed. If this relationship could be demonstrated, continuous monitoring of layer time and thermal gradient could be proposed to provide relevant data to certify the mechanical properties of printed parts without resorting to destructive mechanical testing.

2.2 Mechanical Properties

Standards specifically intended for testing FFF parts and comparing the effect of processing conditions are not yet widespread. As such, researchers still rely on standards intended for classical polymer processing techniques such

as ASTM D638, a versatile test method for tensile properties of plastics. The flat dogbone coupon geometry is readily manufactured using classical processes such as injection or compression moulding. Making them with FFF results in anisotropy, or orientation-dependent properties. As such, multiple orientations must be tested when conducting systematic testing for qualifying materials and processes.

Printing coupons in the Z-direction will highlight the inter-layer bond strength and stiffness. Interlayer tensile strength (or weld strength) is measured using an ASTM D638 coupon printed in the vertical direction. Weld strength is highly dependent on process parameters such as layer height and nozzle temperature which affect the degree of bead coalescence [3].

2.3 Experimental Objective

The objective of this paper is to determine the effect of the inter-layer thermal gradient during the deposition of fused filament on the resulting tensile strength and stiffness. Although the inter-layer tensile strength is one of many mechanical properties which would need to be certified for aerospace part qualification, it was selected for this study due to its expected dependency on processing conditions. Thermal gradient was selected as the parameter to be varied between runs. It is expected to capture the effect of different rates of heat transfer on the development of a strong bond between layers. The print parameters expected to impact thermal gradient are layer time, chamber and extrusion temperatures, print speed, and layer height and width. Layer time was chosen as the parameter to vary between runs due to its wide allowable processing window. Others were held constant to minimize the risk of print failure during trials. The link this paper aims to establish is illustrated in Figure 1.

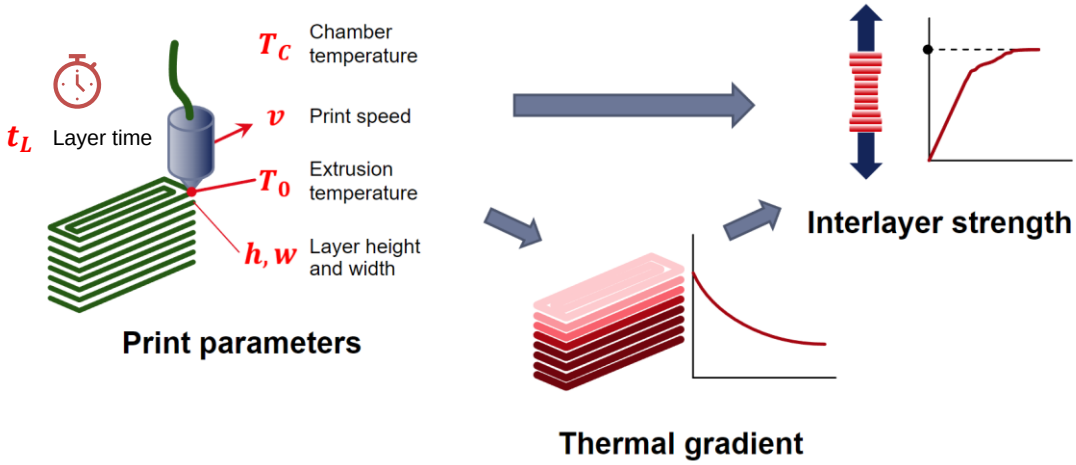

Figure 1: Testing framework to establish a link between print parameters, thermal gradient, and interlayer strength.

3 MATERIALS AND METHODOLOGY

The dependency of weld strength on thermal gradient was evaluated by varying the layer time while printing batches of vertical tensile coupons. Coupon geometry was held constant across trials to purely examine the effect of processing conditions. To vary the layer time without changing the print speed or geometry, coupons were printed simultaneously in batches of different sizes. The material used was ULTEM 9085 filament. Upon reception, the spool was removed from its packaging and dried in a convection oven for 16h at 70°C. It was then immediately loaded into the printer which was maintained at a minimum of 70°C throughout the duration of the experiment.

3.1 Trials

Experimental runs consisted in printing vertical tensile coupons under identical processing conditions, varying only the number of coupons printed at once. Using Fusion360, the coupon geometry was modelled based on the nominal dimensions of an ASTM D638 Type I coupon. The model was imported into Simplify3D in STL format and sliced using the parameters listed in Table 1. Coupons were staggered diagonally in groups of 1, 2, 3, and 4 (Figure 2). Runs were repeated enough times to produce at least 4 coupons each (Table 2).

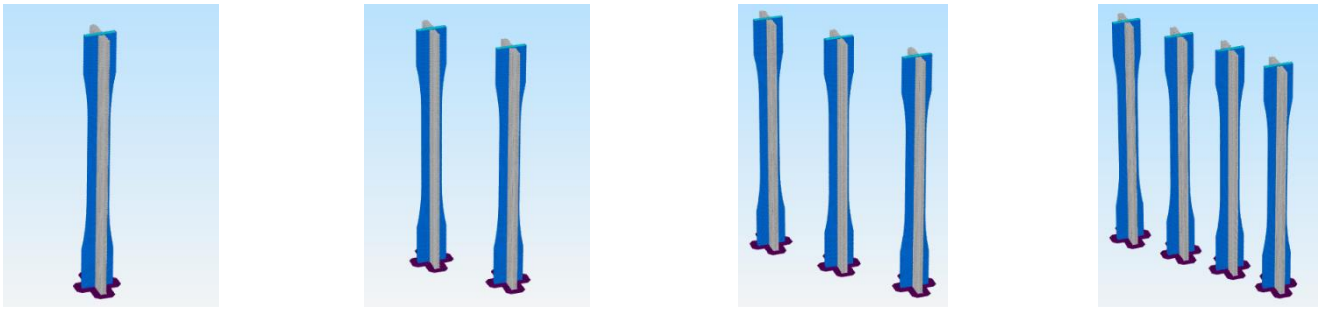

(a) (b) (c) (d)

Figure 2. Experimental runs sliced in Simplify3D: run 1 (a), run 2 (b), run 3 (c), and run 4 (d).

Table 1. Process parameters for printing of vertical tensile coupons.

Parameter	Value
Drying cycle	16h at 70°C
Nozzle temperature	350°C
Bed temperature	180°C
Chamber temperature	120°C
Layer height	0.2 mm
Extrusion width	0.4 mm
Print speed	30 mm/s
Infill density	100%
Infill pattern	Concentric

Table 2. Experimental runs, repetitions, and resulting coupon count.

Run	Coupon Count	Repetitions	Total Coupons
1	1	5	5
2	2	3	6
3	3	2	6
4	4	1	4

3.2 Printer Preparation

Coupons were printed on an AON3D M2 2020 printer. Prior to printing, a thorough preventative maintenance procedure was carried out following the AON3D documentation [4]. The printer was then loaded with a dry spool of filament for coupon printing. Prior to each print, the printer bed and chamber were pre-heated to 180°C and 120°C respectively for 2h. The print area was then probed with the nozzle at 200°C along a grid containing the print area for each run. The nozzle was then heated to 350°C and Nano Polymer adhesive was applied to the print area using a paint brush.

3.3 Coupon Printing and Thermal Monitoring

A single G-code file was created for each run. Parameters in Table 1 were used for each run. Runs were repeated by executing the same file multiple times. The process was closely monitored for the first 2 layers and checked periodically throughout the duration of the print.

A FLIR T420 camera was mounted on a tripod and adjusted to be level with the plane of the nozzle. The mounted camera was positioned near the door latch, 0.8 m away from the print area. Thermograms were captured by opening the door by 0.2 m for 10 to 15 s to capture an image of the print and immediately closing it again. The chamber temperature was recorded before and after the operation. Three thermograms were captured for each print at 30%, 50%, and 70% completion. At each of these points, the layer time was measured using a stopwatch. Upon print completion, coupons were left to rest for at least 15 minutes before being carefully de-bonded from the build plate using a scraper. They were then labelled and transferred to a dry storage cabinet.

3.4 Mechanical Testing

Mechanical testing was conducted on a 100kN Instron electric universal testing machine fitted with tensile grips (Figure 3). Coupons were first dried in a convection oven at 121°C for 48h. Each coupon was measured in length, gauge width, and thickness using a digital caliper. For width and thickness, measurements were taken at 30%, 50%, and 70% of total length and averaged out. Each coupon was then mounted inside the machine and loaded at a rate of 5 mm/min. The machine recorded force as a function of displacement. The failure mode was noted by visual inspection. The Instron software was used to automatically compute Young's modulus and ultimate tensile strength. The strains were calculated based on the crosshead displacement.

Figure 3. Coupon mounted inside the testing machine.

4 RESULTS AND DISCUSSION

The data collected during printing, thermography, and mechanical testing was compiled using Excel and Python. Process data included layer time, ambient temperature and humidity, and chamber temperature before and after capturing the thermograms. Overall, the ambient temperature during the experiment averaged 17.7±0.6°C while relative humidity remained constant at 10%. After each temperature measurement, the chamber temperature dropped by an average of 10.7±7.3°C. This is a source of noise which could have caused the printed coupons to momentarily cool down quicker. It is not expected to have had a significant effect due to the high thermal mass of the coupons. Readings were done three times per print and collected in an Excel table. The PivotTable feature was used to generate Table 3. The average layer time was close to proportional to the number of simultaneous coupons, with deviations due to the additional travel moves required for each additional coupon.

Table 3. Layer time measurements.

Run	Count	Average (s)	Standard deviation (s)
1	15	10.40	0.10
2	18	21.54	0.08
3	18	32.93	0.23
4	12	42.61	0.15

4.1 Thermography Data

Each thermogram was processed in FLIR Thermal Studio. Using the box tool, the coupon temperature field was selected and exported in CSV format. Using Python, entries in each row were averaged out to a single value. The resulting column vector was used to plot the average surface temperature as a function of vertical distance away from the nozzle in pixels (Figure 4). The domain (horizontal span) of each plot is determined by the length of the coupon at the time of measurement.

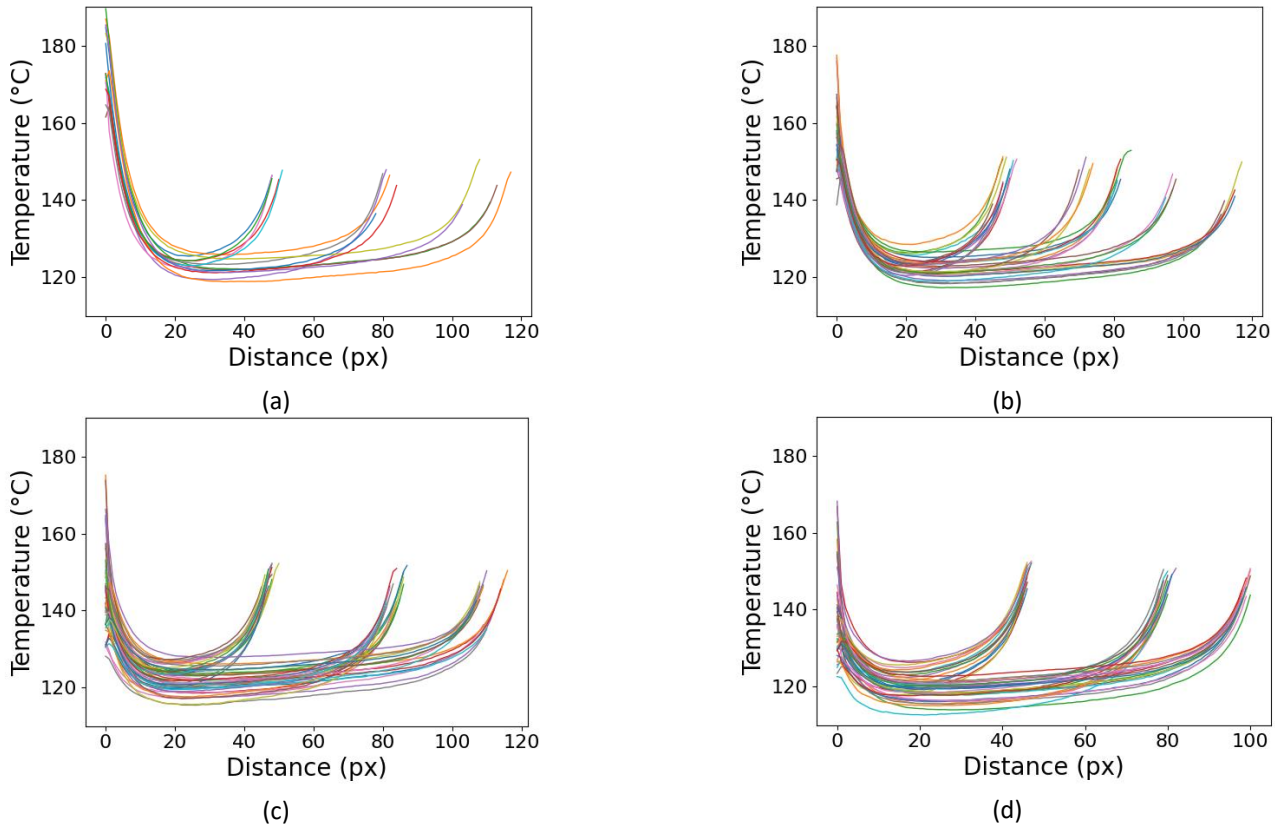

Figure 4. Vertical thermal profiles of coupons printed 1 at a time (a), 2 at a time (b), 3 at a time (c), and 4 at a time (d).

4.2 Mechanical Testing

The Instron software was used to generate a report containing results for tensile testing and dimensional accuracy measurements in CSV and PDF formats. The data was copied to an Excel spreadsheet and analyzed using the PivotTable feature. The average and standard deviation for each property were computed (Table 4, Figure 5).

Table 4. Dimensional accuracy measurements.

Dimension	Count	Average (mm)	Standard dev. (mm)
Thickness	21	3.34	0.03
Width	21	13.09	0.09
Length	21	163.34	0.28

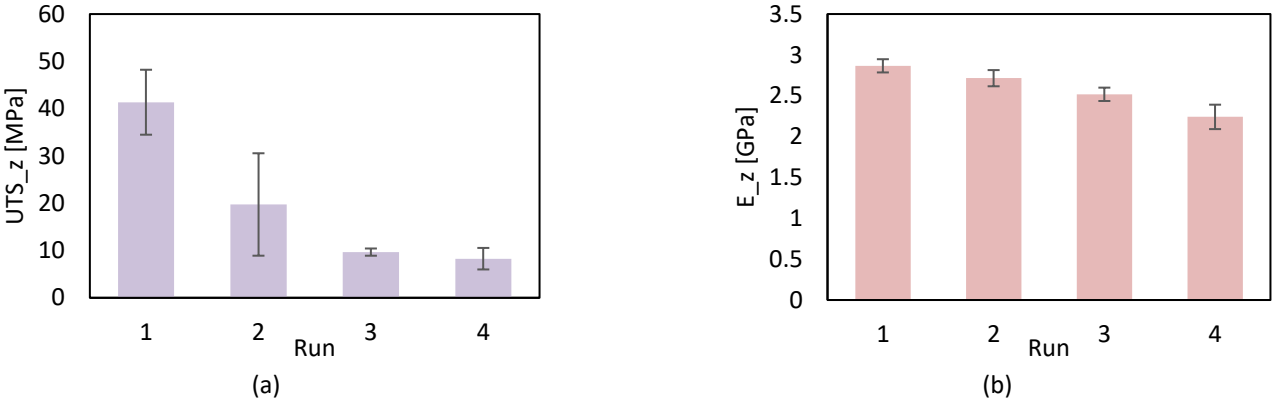

Figure 5. Average ultimate tensile strength (a) and Young's modulus (b) measured for each run.

4.3 Discussion

Thermal profiles were analyzed to determine key process parameters possibly correlated with mechanical properties. The first six points—corresponding to a length of 6.0±0.3 mm or 30.0±1.5 layers—were used to compute the thermal gradient by linear regression. In addition, the top layer and far field temperatures were respectively taken as the initial and minimum value of each profile. Average values for each run are plotted in Figure 6 and Figure 7. By inspection, a gradual decrease was observed in top layer temperature and thermal gradient while far field temperature remains stable across runs. This suggests a correlation between layer time and thermal gradient. This link was verified by one-way analysis of variance (ANOVA) using an alpha of 0.05. Temperature profiles were grouped according to their run (Table 5). The resulting P-value was less than 0.05, indicating a significant difference between the means of each run (Table 6).

Table 5. Summary of thermal gradient data analyzed using ANOVA.

Groups	Count	Sum	Average	Variance
Run 1	15	-89.5	-5.97	0.99
Run 2	36	-151.8	-4.22	1.71
Run 3	51	-152.2	-2.99	2.37
Run 4	47	-113.4	-2.41	2.64

Table 6. ANOVA results.

Source of Variation	SS	df	MS	F	P-value	F crit
Between Groups	177.4	3	59.1	27.3	4.53E-14	2.67
Within Groups	313.7	145	2.16			

As layer time increases, there is a corresponding drop in coefficient of determination, indicating higher variability in thermal gradient measurements. This is attributed to nozzle being in a random position when capturing the

thermogram. The resulting spread in thermal profiles can also be observed in Figure 4c and 4d. Some profiles have a steeper gradient—between -8 and -4°C/px—since they have just received heat from the nozzle. Others have had time to cool down from the previous layer and have gradients between -4 and 0°C/px. Future experiments should account for nozzle position when capturing thermograms, at it is known to significantly impact the instantaneous thermal gradient in addition to overall layer time.

With each measurement, the chamber cooled down by an average of 10.69°C. Since the door was never open for more than 15s, this drop recovered within 2±1 min. and isn't expected to have affected the results. However, this factor makes this method unsuitable for continuous thermal monitoring.

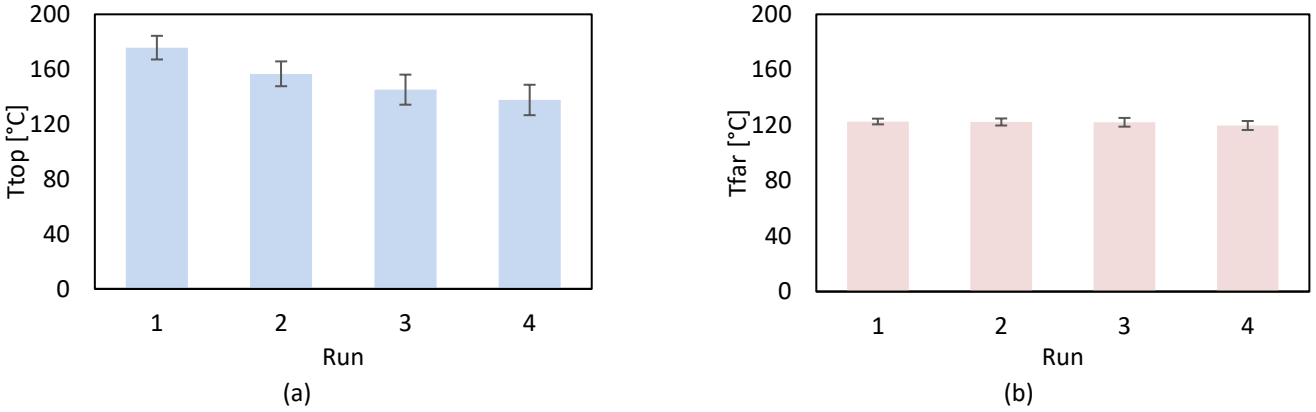

Figure 6. Average top layer temperature (a) and far-field temperature (b) for each run.

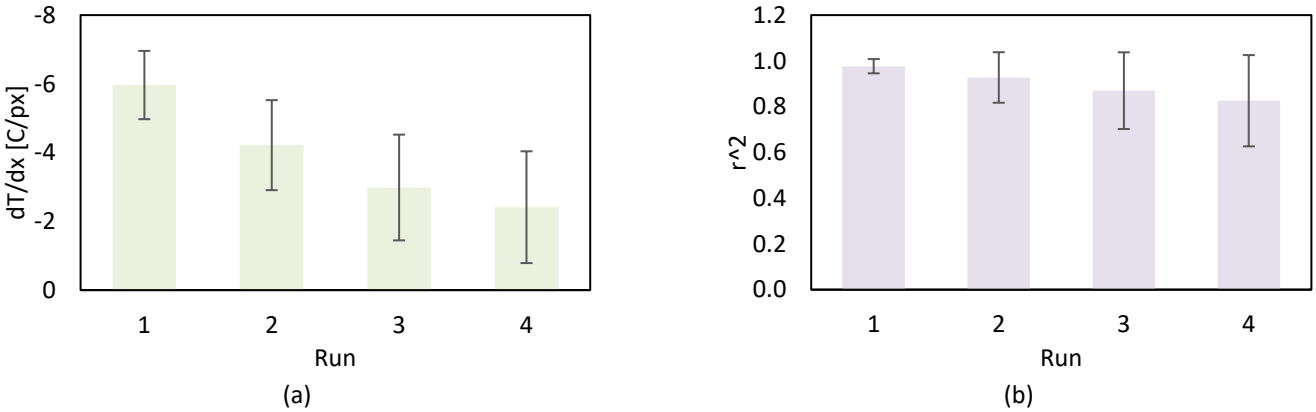

Figure 7. Average thermal gradient (a) and associated coefficient of determination (b).

Mechanical test data indicated an average decrease of 39% in tensile strength and 7.8% in modulus for each additional printed sample. Strength measurements lacked consistency especially for run 2. This is attributed to the nature of the failure mode where the coupon fails at the weakest of all layer interfaces. As such, a higher sample size would be needed to provide reliable strength values.

Increasing the layer time also caused the average top layer temperature to decrease by an average of 7.8% for each additional printed sample. Past studies studying the effect of process temperature on strength only did so for nozzle temperature. Some found that strength was maximized at the highest possible temperature [5, 6] while others found an optimal range [7, 8]. This study is supported by the former two.

5 CONCLUSION

This study found a significant correlation between layer time, thermal gradient, and interlayer tensile strength. It was shown that thermal monitoring can provide valuable data to evaluate and improve part quality. It can provide a full field reading of the print's temperature profile, gradient, and cooldown rate. It could also be used to validate heat transfer models and evaluate the repeatability of the printing process. It could also find applications in deviation feedback based on data or physics-driven models to provide further information on part quality, minimising the need for mechanical testing.

However, there is a challenge in performing thermography while printing materials requiring a heated chamber. Since the FLIR T420 has a maximum operating temperature of 50°C, it cannot be placed inside the 120°C chamber when printing ULTEM 9085. Moreover, the double-pane glass and Lexan (PC) window of the AON3D M2 is IR opaque. As a result, thermal images cannot be captured through it. If continuous monitoring is to be implemented, an apparatus must be developed to either cool down the camera mounted inside the printer or have an IR transparent window to allow the camera to be mounted externally.

The ASTM D638 tensile coupon presents some printability issues but remains the geometry of choice for evaluating the impact of process conditions on mechanical properties. Before an AM-specific coupon is agreed upon, it remains the geometry of choice to evaluate tensile properties in each direction.

6 ACKNOWLEDGEMENTS

The authors gratefully acknowledge the financial support provided by our partners at the Natural Sciences and Engineering Research Council of Canada (NSERC) and PRIMA Québec.

7 REFERENCES

[1] B. G. Compton, B. K. Post, C. E. Duty, L. Love, and V. Kunc, "Thermal analysis of additive manufacturing of large-scale thermoplastic polymer composites," *Additive Manufacturing,* vol. 17, pp. 77-86, 2017/10/01/ 2017.

[2] C. Greer *et al.*, "Introduction to the design rules for Metal Big Area Additive Manufacturing," *Additive Manufacturing,* vol. 27, pp. 159-166, 2019.

[3] AON3D. (2022). *Shrinkage, Residual Stress and Poor Layer Welding in 3D Printing*. Available: www.aon3d.com/material-science/shrinkage-residual-stress-and-poor-layer-welding-in-3d-printing/

[4] AON3D. (2022). *Preventative Maintenance Guide*.

[5] N. Aliheidari, R. Tripuraneni, A. Ameli, and S. Nadimpalli, "Fracture resistance measurement of fused deposition modeling 3D printed polymers," *Polymer Testing,* vol. 60, pp. 94-101, 2017/07/01/ 2017.

[6] C. S. Davis, K. E. Hillgartner, S. H. Han, and J. E. Seppala, "Mechanical strength of welding zones produced by polymer extrusion additive manufacturing," *Additive Manufacturing,* vol. 16, pp. 162-166, 2017.

[7] F. Ning, W. Cong, Y. Hu, and H. Wang, "Additive manufacturing of carbon fiber-reinforced plastic composites using fused deposition modeling: Effects of process parameters on tensile properties," *Journal of Composite Materials,* vol. 51, no. 4, pp. 451-462, 2017/02/01 2016.

[8] S. Berretta, R. Davies, Y. T. Shyng, Y. Wang, and O. Ghita, "Fused Deposition Modelling of high temperature polymers: Exploring CNT PEEK composites," *Polymer Testing,* vol. 63, pp. 251-262, 2017/10/01/ 2017.